Heliyon 10 (2024) e31821

Contents lists available at ScienceDirect

Heliyon

journal homepage: www.cell.com/heliyon

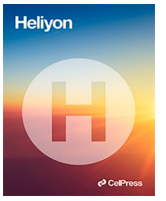

Research article

Effect of human heart valve-derived ECM and NP/PCL electrospun nanofibrous sheet on mice bone marrow mononuclear cells and cardiac repair

Yao Chen [a,c,1,**], Zhanghao Huang [a,b,1], Cheng Ji [a,b], Jia-Hai Shi [a,b,*]

[a] Nantong Key Laboratory of Translational Medicine in Cardiothoracic Diseases, and Research Institution of Translational Medicine in Cardiothoracic Diseases, Affiliated Hospital of Nantong University, Nantong, 226001, Jiangsu, China
[b] Department of Thoracic Surgery, Nantong 226001, Jiangsu, China, Department of Cardiovascular Surgery, Affiliated Hospital of Nantong University, Nantong, 226001, China
[c] Department of Medical Cosmetology, Affiliated Hospital of Nantong University, Nantong, 226001, Jiangsu, China

ARTICLE INFO

Keywords:
Myocardial infarction
BMMNC
hHVS
PCL

ABSTRACT

Background: Biomaterials can improve cardiac repair combined with transplantation of bone marrow mononuclear cells (BMMNCs). In this study, we compared the phenotype and cardiac repair between human heart valve-derived scaffold (hHVS) and natural protein/polycaprolactone (NP/PCL) anchored BMNNCs.
Methods and results: BMMNCs were obtained from mice five days following myocardial infarction. Subsequently, BMMNCs were separately cultured on hHVS and PCL. Proliferation and cardiomyogenic differentiation were detected in vitro. Cardiac function was measured after transplantation of cell-seeded cardiac patch on MI mice. After that, the BMMNCs were collected for mRNA sequencing after culturing on the scaffolds. Upon anchoring onto hHVS or PCL, BMMNCs exhibited an increased capacity for proliferation in vitro, however, the cells on hHVS exhibited superior cardiomyogenic differentiation ability. Moreover, both BMMNCs-seeded biomaterials effectively improved cardiac function after 4 weeks of transplantation, with reduced infarction area and restricted LV remodeling. Cell-seeded hHVS was superior to cell-seeded PCL.
Conclusion: BMMNCs on hHVS showed better capacity in both cell cardiac repairing and improvement for cardiac function than on PCL. Compared with seeded onto PCL, BMMNCs on hHVS had 253 genes up regulated and 189 genes down regulated. The reason for hHVS' better performance than PCL as a scaffold for BMMNCs might be due to the fact that optimized method of decellularization let more cytokines in ECM retained.

1. Introduction

Myocardial infarction, a pathological phenomenon occurring in myocardial tissue, can lead to cellular injury and mortality. Ischemia arises when the blood flow to an organ is impeded due to an embolus obstructing the arterial blood supply. This ischemic

* Corresponding author.
** Corresponding author.
E-mail addresses: doctorcy@ntu.edu.cn (Y. Chen), sjh@ntu.edu.cn (J.-H. Shi).
[1] These authors contribute equally to this work.

https://doi.org/10.1016/j.heliyon.2024.e31821
Received 14 October 2022; Received in revised form 6 April 2024; Accepted 22 May 2024
Available online 24 May 2024

event is associated with a significant disruption in cellular metabolism, ultimately leading to tissue hypoxia. Within the affected ischemic region, excessive tissue damage and detrimental inflammation are observed [1]. Myocardial infarction is a pathological process that occurs in myocardial tissue and can cause cell damage and death. Ischemia occurs when the blood supply to an organ is restricted due to an embolus blocking the blood supply of an artery. During the occurrence of acute myocardial infarction (AMI), a significant quantity of inflammatory cells is mobilized into the myocardium. Neutrophils engulf deceased and dying cells in the affected region and subsequently release inflammatory mediators to attract monocytes. As the acute inflammatory response commences resolution, the majority of infiltrating neutrophils undergo apoptosis. Inflammatory macrophages eliminate apoptotic neutrophils, initiating a sequence of anti-inflammatory pathways that facilitate cardiac repair [2]. Defective neutrophil clearance enhances inflammation and promotes cardiomyocyte apoptosis, infarct dilation, and adverse structural remodeling [3]. Intramyocardial transplantation of bone marrow undifferentiated cells can repair the infarcted heart through angiogenesis, paracrine effects, transdifferentiation and cell fusion. Our research found that both cardiac and bone marrow derived cell population is increased in response to ischemic injury and can improve cardiac repairing as well as increased chemotaxis to the heart [4].

However, the survival rate of cells injected into the myocardium locally is significantly diminished due to the majority of cells being lost through mechanical damage, and the remaining cells experiencing death within a week of transplantation due to inadequate nutrient and oxygen provision [5]. In order to tackle this issue, we propose the provision of cells with an environment that closely resembles their native surroundings, specifically the cardiac extracellular matrix (ECM), which has the potential to enhance their viability and proliferation rates. Therefore, the implementation of a cardiac extracellular matrix (ECM) that accurately reproduces the structural attributes and biochemical composition of the indigenous milieu can yield significant benefits. Consequently, the provision of a cardiac ECM that emulates both the structural characteristics and biochemical composition of the native myocardial ECM promotes successful myocardial transplantation [6]. The utilization of hybrid nanofibers produced through electrospinning technology, incorporating diverse natural proteins, enhances cell adhesion and spreading on the scaffold. Furthermore, the utilization of human native myocardial tissue-derived matrix may provide a clinically relevant novel scaffold and support for BM stem cell transplantation in cardiac repair holds significant clinical relevance. The objective of our research was to conduct a comparative analysis between these two materials and the original microenvironment of the myocardium, with the aim of determining their respective levels of biocompatibility and ability to simulate the cardiac microenvironment. By identifying the reasons behind the superior performance of one material over the other, we can facilitate the development of improved materials that more accurately replicate the cardiac microenvironment, thereby enhancing the efficacy of cardiac repair procedures.

2. Materials and methods

2.1. Preparation of hHVS

The human mitral valve was derived from a patient with chordal rupture undergoing mitral valve replacement in the Affiliated Hospital of Nantong University as described in Ref. [6]. The mitral valve was frozen sectioned to a thickness of 50 μm or 100 μm, followed by decellularization in 0.5 % or 1 % sodium dodecyl sulfate (SDS) (the thickness of the scaffold determines the concentration) for 12 h. The decellularized hHVS was washed repeatedly before freeze-drying in a vacuum freeze dryer to remove residual SDS, then immersed it in 75 % ethanol for 2 h.

2.2. Synthesis and characterization of electrospun sheet

PCL and NP are mixed in a ratio of 8:2. Elastin (Herochem Biochemical reagent CO. LTD, China) and type I collagen (Sigma, US) are made into natural protein with a mass ratio of 3:7. The mixture was dissolved in hexafluoroisopropanol (HFIP) (Aladdin, China) and stirred for 12 h to obtain a uniform and stable solution with a mixed solvent concentration of 15 % (w/v). The prepared solution is loaded in a 2 ml container, and the flow rate of the solution was controlled by the syringe pump at 0.02 ml min^{-1} (LSP01-1A, Baoding Longer Precision Pump, China). The needle tip was 12.5 cm away from the current collector, and the voltage applied to the needle was 15v. The prepared electrospun sheet was vacuum dried for 24 h to completely remove the residual solvent, and then used for further characterization. All experiments are carried out at room temperature and relative humidity between 40 and 60 %. Scanning electron microscope (SEM) was used to observe the morphology of NP/PCL (abbreviated as PCL in following text) electrospun sheet. ImageJ® software was used to measure 100 fiber segments in different SEM images to determine the average fiber diameter. Measured the water contact angle (WCA) of the electrospun sheet by the fixed drop method, using a goniometer that supports video ((FM40MK2 EasyDrop, KRÜSS GmbH, Germany) [7].

2.3. Development of MI model

All C57BL/6 or GFP + transgenic mice (6–8 weeks, 20–25g) used in this study were purchased from the Model Animals Research Center of Nantong University (Nantong, China). GFP + transgenic mice were used for transplanted cells tracking. Mice were housed in a specific pathogen-free (SPF) environment at 22 ± 1 °C with a relative humidity of 50 ± 1 % and a normal 12-h day–night cycle. After the mice were anesthetized with isoflurane inhalation, a small incision was opened in the left chest, the muscle tissue was bluntly separated, and the left descending artery (LDA) was ligated with 7-0 propylene after the heart extrusion exposure. After that, removed possible gas from the chest, cleaned the wound, sutured and disinfected [8,9].

2.4. Extraction and culture of BMMNCs

Fresh BMNNCs was isolated by washing the femoral and tibial bone marrow of C57BL/6 or GFP + mice with myocardial infarction with Hank's balanced salt solution with 40 μm cell strainer (HBSS; Thermo, USA). The collected cells were cultured in dulbecco's modified eagle medium (DMEM) supplemented with 15 % fetal bovine serum (Gibco, Thermo, USA) and 1 % penicillin-streptomycin solution (P/S, Thermo, USA). HHVS and PCL electrospun sheets were placed on the bottom of the 96-well plates. BMMNC cells were then seeded in 96-well plates and culture performed in humidity incubator at 37 °C and 5 % CO_2 for proliferation and PCR tests. The cell-seeded hHVS and PCL was prepared by incubating the hHVS or PCL in the medium by growing BMMNC cells (3×10^5 cells/cm^2) onto the materials for 10 days, respectively, before implantation.

2.5. Transplantation of the materials

Thirty-seven C57BL/6 mice were randomly assigned to 5 groups: 1) Sham group (n = 7); 2) MI group (n = 10); 3)BMMNC-seeded PCL group (n = 10); 4) BMMNC-seeded hHVS group (n = 10). Surgical anesthetization and method of exposure of mice hearts of transplanting cardiac patches were the same as MI surgery. Once the pericardium was opened, a 7-0 prolene, which was sutured in advance in the sheet, was utilized to ligate the LDA. Hereafter, the sheet was set to the left ventricle. The sheet attached to the epicardium without using glue.

2.6. Evaluation of cardiac function

After four weeks of implantation, transthoracic echocardiography (LG, South Korean) and pressure-volume (P/V) loop measurements (using the Millar Pressure-Volume System) were conducted on recipient mice to assess cardiac performance, as previously described [10]. Briefly, Two-dimensional and M-mode images were recorded from the short-axis view of the 4th to 5th intercostal space in the middle of the left ventricle. In order to evaluate cardiac function, ejection fraction (EF) and fraction shortening (FS) are automatically generated by the machine. All measurements were performed by experienced sonographers, who were unaware of the grouping of mice [11–13]. In vivo hemodynamic analysis was carried out using a 1.4F pressure-volume catheter (SPR-839) [14,15].

Measured a set of hemodynamic parameters to determine the systolic and diastolic blood pressure of the heart. The mice were anesthetized using an isoflurane inhalation chamber. After calibration, inserted the probe into the left ventricle from the left common carotid artery, and the left ventricular pressure and conductance was obtained in real time. Subsequently, a 20 % sodium chloride solution was injected intravenously 3 times. After correcting the volume data by conductance measurement, the mice were sacrificed for tissue collection [16,17]. Statistical analyses were performed using *PRISM* (*GraphPad* Software Inc) with the non-paired *t*-test.

2.7. High-throughput sequencing data analysis

This project uses RNA Extraction kit to extract RNA from samples. The cell-sheet complex was in RNA Extraction lysate. The extraction strictly follows the standard operation manual provided by the kit manufacturer, and the extracted total RNA of the samples is obtained.

The total RNA extracted was tested by Agilent Bioanalyzer 2100 (Agilent technologies, Santa Clara, CA, US) to detect the integrity of RNA.Qubit®3.0 Fluorometer (Life Technologies, CA, USA) and Nanodrop One spectrophotometer (Thermo Fisher Scientific Inc., USA) to detect the concentration and purity of total RNA.For details about the quality inspection result, see the Quality inspection report.

Aftering sequencing on the Illumina HiSeq4000 sequencer, paired-end reads were harvested and these were quality controlled by Q30. The clean data were obtained through 3' adaptor-trimming and removing low-quality reads usingcutadapt software (v1.9.3). After that, clean data were aligned to the reference genome (mmu) via software HISAT2 (v2.0.4). Methylated sited on lncRNAs (peaks) were identified by MACS software. As to the mRNA and lncRNA part, clean reads were aligned to the human reference genome (UCSC hg19) with HISAT2 software (v2.0.4). Then, low expressed genes were filtered out for further analysis.

2.8. Detection of differential expressed genes

The differential gene expression between groups was determined by edger and DEseq2 R package. Genes with a cutoff of p-value$<$0.05 and $|\log2\ (\text{foldchange})| \geq 1$ or 0.58 were considered differential expressed.

2.9. Functional enrichment analysis

The Kyoto Encyclopedia of Genes and Genomes (KEGG) database and Gene Ontology (GO) category database were used for functional annotation of differentially expressed genes. Enrichment analysis of GO categories was performed by R 'cluster Profiler' package, and enrichment analysis of pathways was tested upon hypergeometric distribution by R 'phyper' function. Those GO categories with a fdr$<$0.05 were considered as significant enriched, and pathways with a p-value$<$0.05 were considered as significant enriched [18,19].

2.10. Gene set enrichment analysis

Gene set enrichment analysis (GSEA) was used to interpret the gene expression data by determining statistically significant differences in pre-defined gene-sets between biological states. In addition, GSEA can be used to identify the pathways that correlate to gene expression. The predefined gene set for mouse were downloaded from GO2MSIG (http://www.bioinformatics.org/go2msig/). A normalized enrichment score (NES) was calculated as the primary GSEA statistic. Gene sets were considered signifcantly enriched with p-values<0.05 and $|NES|\geq 1$. These analyses were done by R 'fgsea' package [20–22].

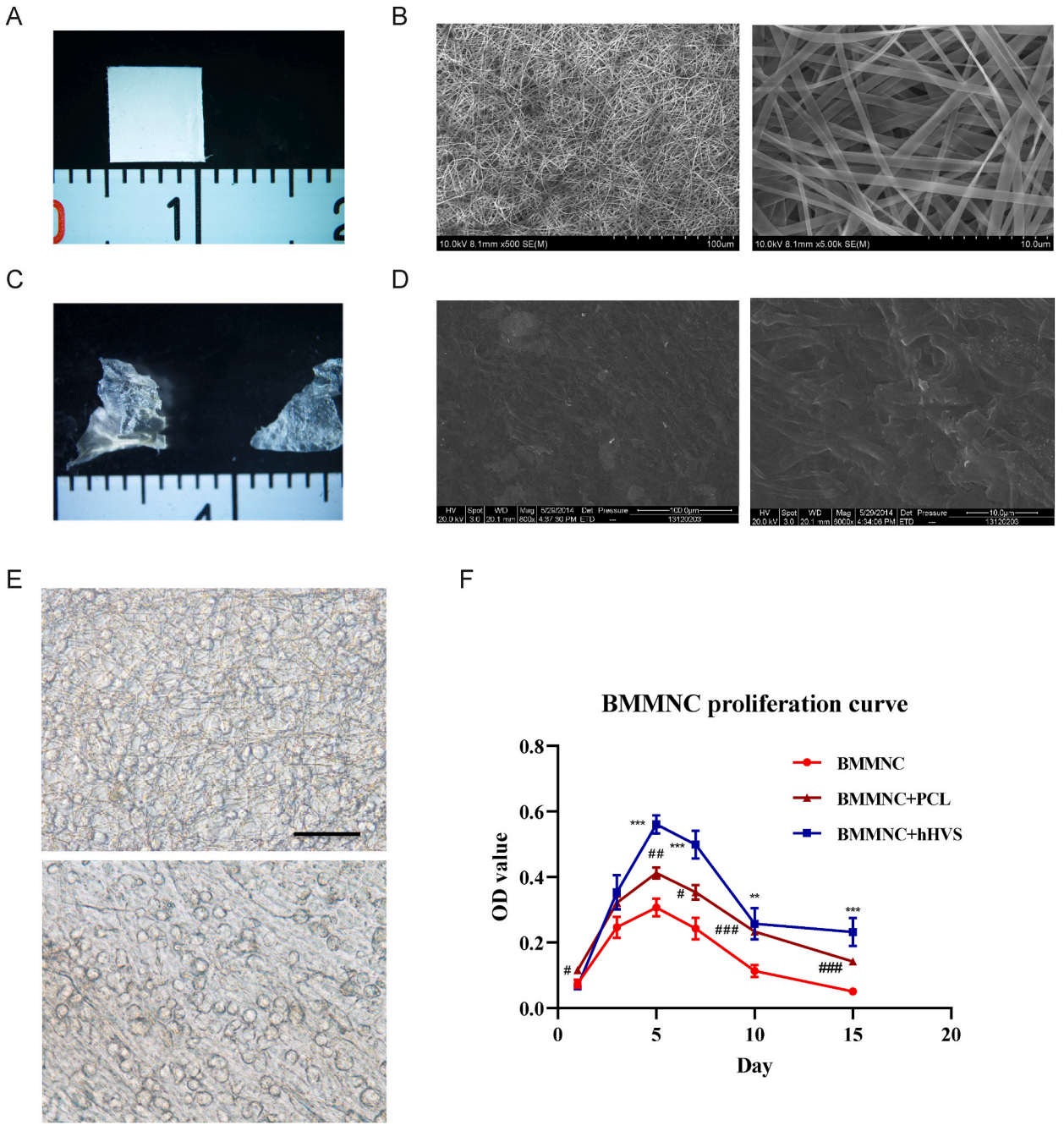

Fig. 1. Features of the Heart Patch (A) Macroscopic view of 100 μm PCL sections. (B) Scanning of 100 μm PCL for electron microscopy (1000x, 6000x). Scan bar, 20 μm. (C) Macroscopic view of 100 μm hHVS sections. (D) Scanning of 100 μm hHVS after decellularization for electron microscopy. (E) Expression of proliferation-related proteins in BMMNC and two cardiac patches. (F) Cck8 is used to show the proliferation of BMMNC cells themselves and their ability to proliferate on PCL and hHVS respectively.

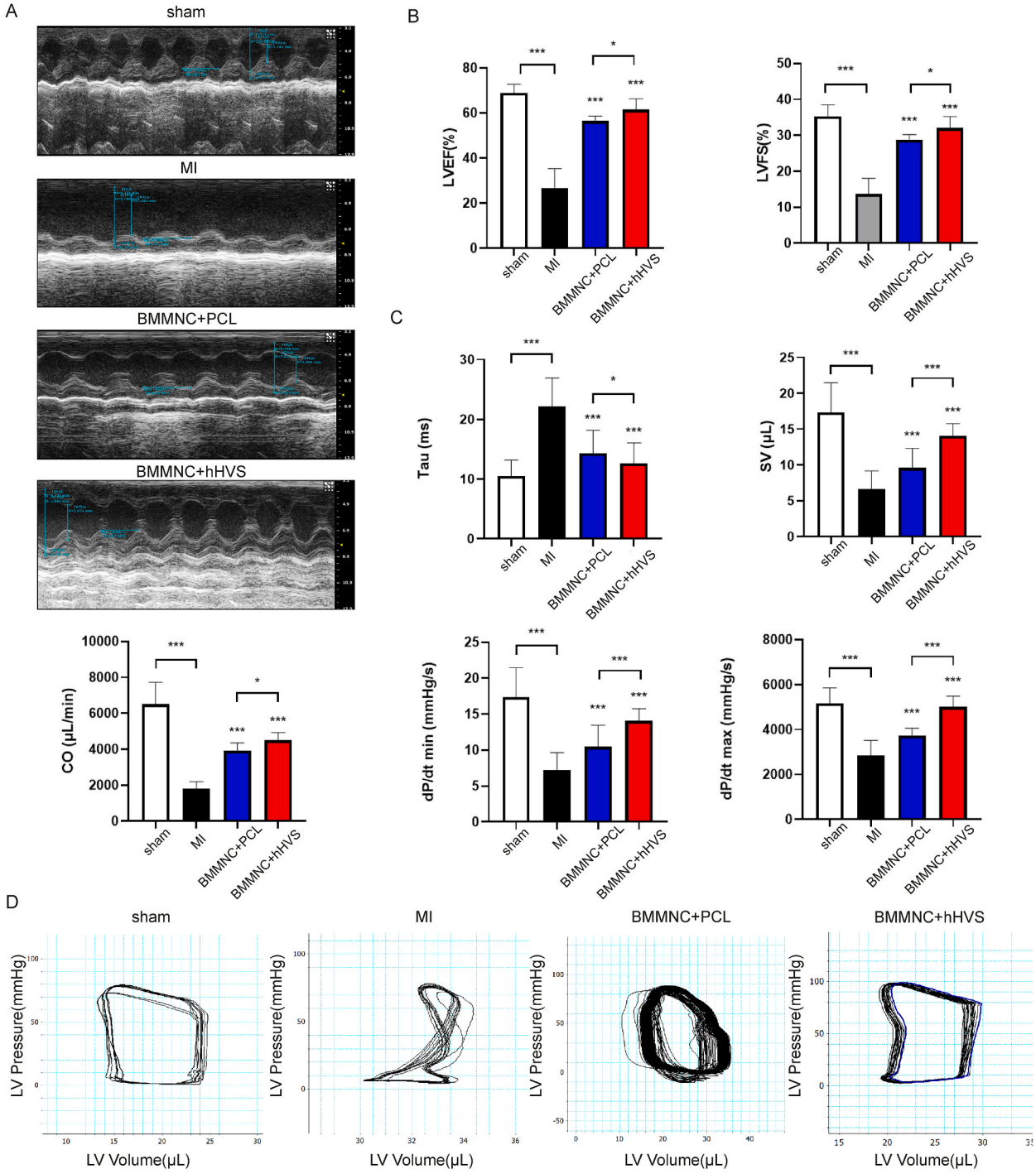

Fig. 2. Cardiac function testing (A–B) Echocardiography is used for the detection of cardiac function in mice, and the indices of cardiac function detected include LVEF and LVFS. (C-D)Haemodynamic measurements via Millar pressure-volume catheter. The calculated haemodynamic parameters are shown as pump function (cardiac output, CO; output per beat, SV), systolic function (maximum peak rate of LV pressure, dP/dt max) and diastolic function (LV pressure rate in minimum peak MI, dP/dt min; relaxation time constant, Tau). Each loop represents one cardiac cycle. MI, n = 10; hHVS + BMMNC, n = 10; NORMAL, n = 7.

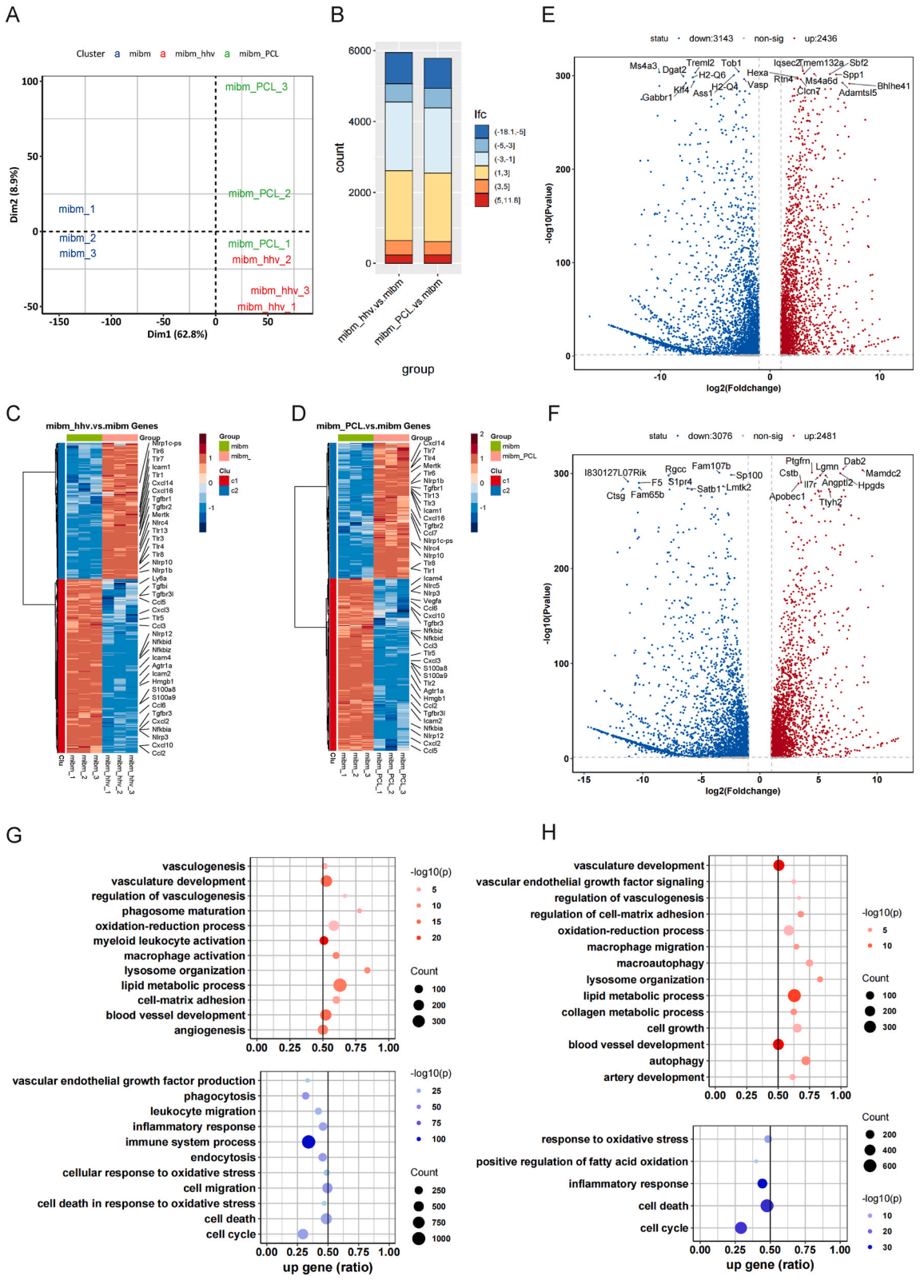

(caption on next page)

Fig. 3. Similarities between hHVS and PCL (A) PCA and sample hierarchical cluster analysis were performed on the normalized expression values of the 3 groups of samples. The results showed that the samples in the same group were very similar. The PCL and hHVS samples are still significantly different from the mibm samples. The similarity between hHVS and PCL is reflected in the fact that the horizontal coordinate is located in the similar region (Dim1), while the difference is reflected in the inconsistent distribution of the two on the vertical coordinate (Dim2). (B) Histogram display of the number of differential genes. The color of the histogram is gradually filled according to the change interval of the log2 Foldchange value of the difference gene. Red represents up, blue represents down, and the depth of the color represents the degree, and the ordinate is used to display the number of distributions. (C) Heat map of differential genes between hHVS and BMMNC planted with BMMNC, red represents high expression, blue represents low expression, the darker the color, the deeper the degree. (D)Heat map of differential genes between PCL and BMMNC planted with BMMNC, red represents high expression, blue represents low expression, the darker the color, the deeper the degree. (E) Differential gene volcano maps of PCL and hHVS compared with mibm. Each row represents a gene, each column represents a sample; Genes are clustered row by row. (F) Differential gene volcano map of PCL and hHVS compared with mibm. The horizontal axis represents log2 Foldchange, and the vertical axis represents -log10 (Pvalue). The more the gene is at the top, the more obvious the difference between the left and right sides. Among them are the top 20 significantly different genes ranked by pvalue significance. (G–H) The result of functional enrichment of differentially expressed genes. Each dot represents a biological function, and the size of the dot reflects the number of differential genes in this function; the shade of the dot reflects the size of -log10(pvalue). The horizontal axis represents the ratio of up-regulated genes to down-regulated genes in this function. (For interpretation of the references to color in this figure legend, the reader is referred to the Web version of this article.)

2.11. Protein microarray results analysis

The protein-protein interaction between DEGs were extracted based on Pathway common database (http://www.pathwaycommons.org/). Both the PCL and hHVS differential genes (DEGs) compared with mibm were used, and protein-protein interaction (PPI) network were created seperatly. As to each gene in the network, we calculated its betweeness score, and compared it in two networks. A gene with a betweeness score higher than log2 fold change between two networks was considered as one network specific hub genes [23].

3. Results

3.1. Characterization of PCL and hHVS

Electrospun sheet was made from a blend of 80 % elastin and PCL (Fig. 1A). The electrospun sheets showed a porous, dense and uniform morphology under scanning microscopy (Fig. 1B). HHVS were made from a decellularized valve (Fig. 1C). After decellularization, the scanning electron microscope showed interconnected porous meshes, indicating a well-preserved fine nanofibre network structure (Fig. 1D). To further confirm the adhesion between cells and scaffolds, we grew BMMNCs extracted from mice onto PCL and hHVS for 7 days and observed by electron microscopy that BMMNC cells survived and adhered well on both PCL and hHVS (Fig. 1E) [24,25]. To further investigate the proliferation of BMMNCs, we compared the proliferation of BMMNCs grown on PCL and hHVS. BMMNCs grown on PCL and hHVS proliferated more strongly compared to the proliferation ability of BMMNCs themselves. In addition, BMMNCs grown on hHVS proliferated more strongly than BMMNCs grown on PCL (Fig. 1E).

3.2. PCL and hHVS implanted with BMMNC significantly improve cardiac function

Compared to the sham group, the infarcted mice showed a significant decrease in LVEF and LVFS, whereas the mice with PCL and hHVS in the infarcted area showed a significant increase in LVEF and LVFS. It is also noteworthy that cardiac function improved better in mice with hHVS than in mice with PCL (Fig. 2A-B). To further assess the effect of these heart patches on the heart, hemodynamic measurements were monitored by Millar catheter in mice after one month. Compared to the sham-operated group, the dp/dt, CO, and SV of the infarcted mice were significantly lower and the Tau was significantly higher, while the dp/dt, CO, and SV were significantly restored and the Tau was significantly lower after applying the two heart patches. The effect of hHVS was more pronounced than that of PCL. The lines become regular when PCL and hHVS are applied, as opposed to the haphazard lines on the post-infarction loop chart (Fig. 2C-D).

3.3. Similarity of cardiac patch hHVS to PCL

Principal component analysis (PCA) and sample level clustering analysis showed differences between the three sample groups, with significant differences between the two heart patch groups and the infarct group, and very high sample similarity in each group (Fig. 3A). Interval classification of the differential genes in the two groups of heart patches according to the values of |log2(foldchange| showed a very high similarity in the distribution of the differential genes in the two groups (Fig. 3B). Heat map showing differential genes between the hHVS and BMMNCs groups of heart patches implanted with BMMNCs (Fig. 3C), while differential genes between the PCL and BMMNCs groups of heart patches implanted with BMMNCs are shown by Fig. 3D. Volcano plots showed 3143 down-regulated genes compared to 2436 up-regulated genes in the hHVS group compared to the infarct group, and 3076 down-regulated genes compared to 2481 up-regulated genes in the PCL group compared to the infarct group (Fig. 3E-F) (Fig. S1). The functional enrichment analysis of the differential genes in the two groups of heart patches was similar, with upregulated genes in the same pathways being mainly in vasculature development, regulation of vasculogenesis, oxidation-reduction process, lysosome. The

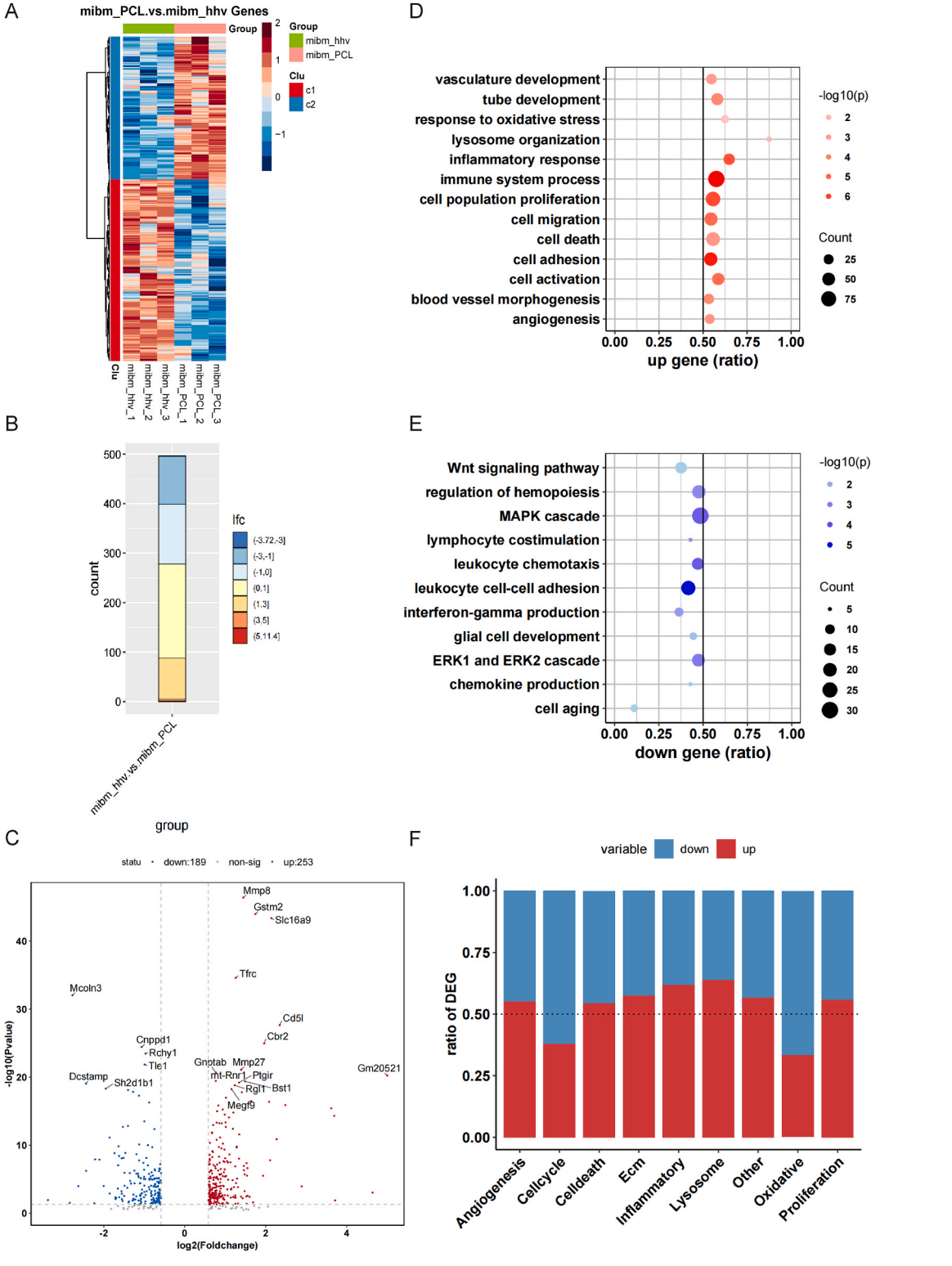

(caption on next page)

Fig. 4. Differences between hHVS and PCL (A) Differential gene heat maps of hHVS compared with PCL. (B) Histogram display of the number of differential genes. Different colors represent the distribution of logfoldchange values in different segments, and the ordinate is used to display the number of distributions. (C) Volcano map of differential genes compared between PCL and hHVS; there are a total of 253 up-regulated and 189 down-regulated; among them, the top 20 significantly different genes ranked by pvalue significance. (D–E) Functional enrichment of differentially expressed genes of hHVS and PCL. (F) The proportional distribution of differential genes related to specific biological functions. Red represents up-regulated expression in hhv, and blue represents down-regulated expression. (For interpretation of the references to color in this figure legend, the reader is referred to the Web version of this article.)

pathways with the same up-regulated genes were mainly the fasculature development, regulation of vasculogenesis, oxidation-reduction process, lysosome organization, lipid metabolic process, and blood vessel development (Fig. 3G-H) [26].

3.4. Differences between cardiac patch hHVS and PCL

The heat map shows the differential genes between hHVS and PCL (Fig. 4A), the bar chart showed the distribution of log2 fold-change for the differential genes between the two heart patches (Fig. 4B), and the volcano chart indicates that there were 189 down-regulated genes and 253 up-regulated genes between the two groups (Fig. 4C). The functional enrichment of the differential genes showed significant differences in cell proliferation, inflammation-related and angiogenesis between the two heart patches (Fig. 4D and E). The respective percentages of up- and down-regulated differential genes in the significantly enriched pathways were shown in the bar chart (Fig. 4F). The differential genes were mainly enriched in angiogenesis, inflammatory, ECM and proliferation, suggesting that BMMNCs grown on hHVS are beneficial in mimicking the cardiac microenvironment compared with BMMNCs grown on PCL.

3.5. Differential gene-specific differential enrichment of two cardiac patches

The hHVS equivalent of the PCL heart patch had 602 specific differential genes, of which there were 311 up-regulated differential genes and 291 down-regulated differential genes. In contrast, PCL compared to hHVS heart patch had 438 specific differential genes, of which there were 246 up-regulated differential genes and 192 down-regulated differential genes (Fig. 5A). The genes specific to the cardiac patch hHVS were mainly enriched in macromolecule localization and cellular compared to PCL, whereas the genes specific to the cardiac patch PCL were mainly enriched in phosphate-containing compound metabolic process and macromolecule localization compared to hHVS (Fig. 5B-C). The pathways of differential gene enrichment positive by each of the two cardiac patches were shown in the deviation diagram (Fig. 5D). The negative part of the differential gene enrichment pathway of the two heart plaque modulation also indicates the similarity between the two, while the positive part indicates the difference between the two. In GSEA enrichment analysis, hHVS compared with PCL, the up-regulated specific differential genes were mainly enriched in cell proliferation involved in heart morphogenesis, vasculogenesis, cell adhesion, coronary vasculature morphogenesis, and lysosome organization, while the down-regulated specific differential genes were mainly enriched in steroid biosynthetic process (Fig. 5E) [27].

3.6. The superiority of the cardiac patch hHVS

The heat map focused on the differential genes associated with PCL and hHVS in terms of proliferation, cell death and immunity (Fig. 6A-C). Histograms of the up- and down-regulation of the respective hub genes in the PPI network constructed from some of the differential genes; it can be seen that both hHVS and PCL hub genes are biased towards up-regulation of expression in hHVS (Fig. 6D). The protein chip consisted of normal valves and decellularised valves. We found that the decellularised valves still secrete growth-like factors, inflammatory factors and extracellular matrix-related factors (Fig. 7A-B). The proteins that remaind in higher amounts after decellularization of the valve are angiogenin, VEGF, IL-1B and TIMP1. Angiogenin had a strong ability to promote angiogenesis both in vivo and in vitro. VEGF is a highly specific pro-vascular endothelial cell growth factor that promotes increased vascular permeability, extracellular matrix degeneration, vascular endothelial cell migration, proliferation and angiogenesi. TIMP1 is a group of peptidases involved in the degradation of the extracellular matrix and promotes the proliferation of many cell types and may also have an anti-apoptotic function. IL-1B is a key pro-inflammatory cytokine that has been associated with the development of atherosclerosis and myocardial infarction. We also enriched myocardial valves for residual proteins and found that residual proteins were mainly enriched in cell adhesion, angiogenesis, and immune-related pathways (Fig. 7C). The reciprocal and downstream genes corresponding to the residual proteins are presented on the network map. The main residual proteins were TNF-α, IL-1b, TIMP-1, MMP1. The yellow diamond-shaped dots were residual proteins, the red dots were adhesion-related genes and the blue dots are genes for other biological functions. The red and blue dots were residual proteins corresponding to interacting or downstream genes and differentially expressed in PCL compared to hHVS (Fig. 7D).

4. Discussion

In our previous investigation, it was observed that the utilization of materials combined with BMMNC cells demonstrated a significantly greater efficacy in enhancing cardiac repair compared to the use of materials alone [28]. In the present investigation, we aimed to compare the effectiveness of two heart patches cultivated with BMMNC cells in improving myocardial repair. The current limitations of differentiated cell-based cardiac regenerative therapies lie in the inefficiency of cell delivery, engraftment, and differentiation within the myocardium following transplantation. Furthermore, the extracellular matrix (ECM) undergoes alterations during

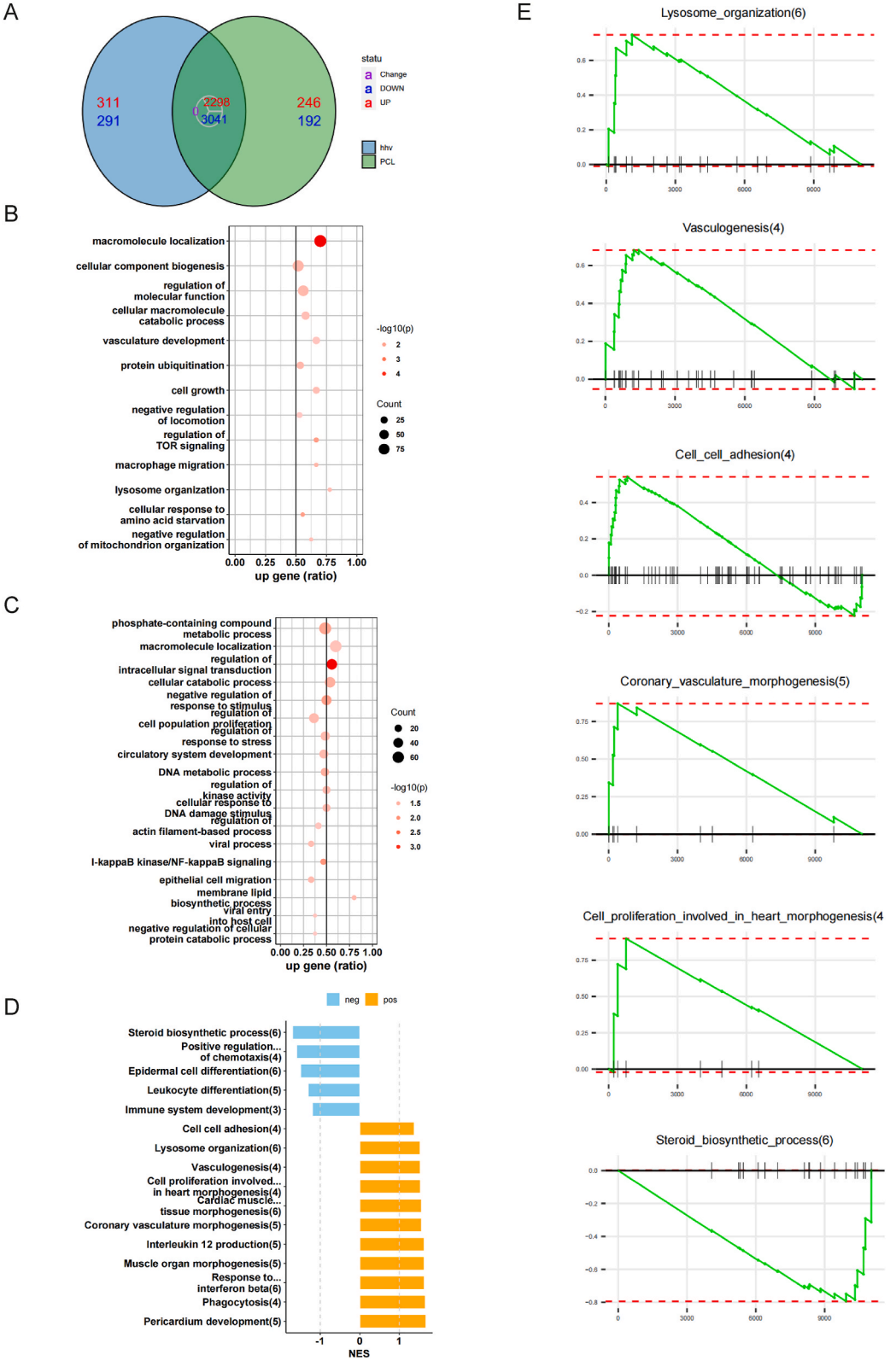

(caption on next page)

Fig. 5. Intentional differences between hHVS and PCL. (A) The venn diagram shows the intersection of differential genes between PCL and hHVS compared with MI. The figure is filled in according to the following categories: red represents up-regulation, blue down-regulation; purple up-regulation is in the opposite direction; most of the genes appear to be up-regulated together, and no genes have the opposite trend. (B) The result of functional enrichment hHVS are significantly enriched in cell growth and other pathway. (C) The result of functional enrichment of specific differentially expressed genes in PCL. Genes with specific differences in PCL are significantly enriched in metabolic and signal transduction pathways. (D) GSEA analysis result of hhv and PCL comparison (bp). All results satisfy $p < 0.05$. The horizontal axis reflects the Normalized enrichment score (NES) value. NES>1 means that HHV is up-regulated compared to PCL, and NES<1 means that hHVS is down-regulated compared to PCL. (E) The curve of the distribution of the biological function Enrichment score value. Cell proliferation involved in heart morphogenesis, vasculogeneis, cell adhesion, and lysosome are significantly up-regulated in hHVS genes. Steroid is down-regulated in the PCL group. (For interpretation of the references to color in this figure legend, the reader is referred to the Web version of this article.)

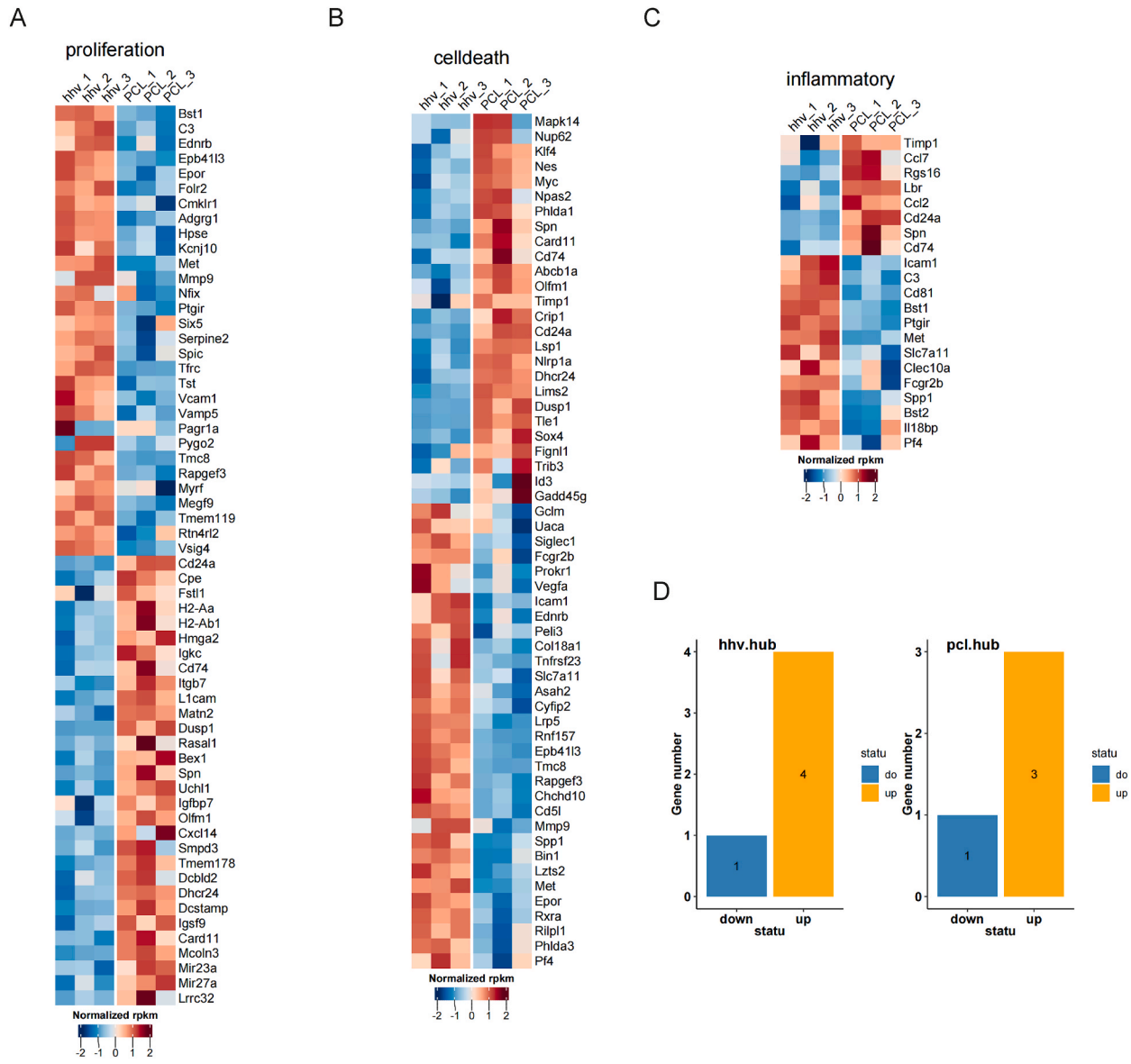

Fig. 6. Differential analysis of hHVS and PCL in specific pathways. (A) Heatmap expression of differential genes between hHVS and PCL in the proliferative pathway. (B) Heat map expression of differential genes between hHVS and PCL in the cell death pathway. (C) Heat map expression of differential genes between hHVS and PCL in the immune pathway. (D) Histogram of the up- and down-regulation of the respective hub genes of PCL and hHVS.

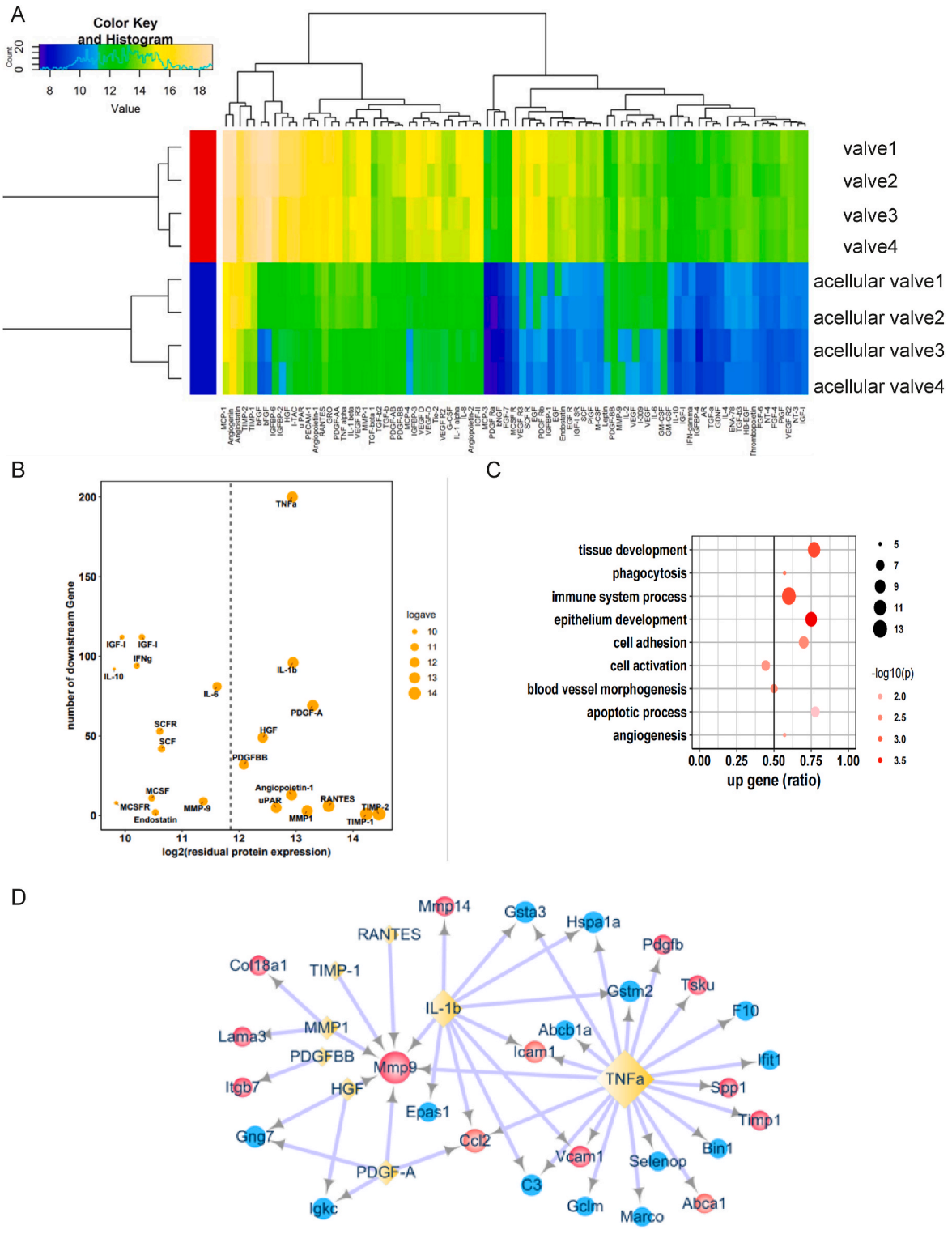

Fig. 7. Advantages of hHVS (A) Protein chip heat map. Yellow represents high expression, blue represents low expression, and green is somewhere in between. (B) The horizontal axis is the residual protein expression data, and the vertical axis is the number of downstream proteins or genes of the corresponding protein. The size of the dot reflects the amount of residual protein expression, the larger the value, the larger the dot. The dotted line is the median value of residual protein expression. The residual protein expression is greater than the residual protein at the position of the dotted line, which is considered to have an impact on the follow-up. (C) The result of functional enrichment of downstream genes of residual protein. (D) Protein interaction network. The yellow diamond-shaped dots are residual proteins, the red dots are adhesion-related genes, and the blue dots are

genes for other biological functions. The red and blue dots are the residual protein corresponding to the interaction or downstream genes and are differentially expressed in hHVS and PCL. (For interpretation of the references to color in this figure legend, the reader is referred to the Web version of this article.)

the progression of heart failure, leading to its substitution with scar tissue. This substitution exacerbates the decline in the survival rate of transplanted cells. Consequently, tissue engineering using different biomaterials and cell types was being developed as a potential therapeutic approach to improve the efficiency of stem cell therapy by increasing the survival and retention of transplanted cells.

The naturally decellularized ECM not only serves as a physical framework to uphold the structural integrity of a multicellular organism but also functions as a reservoir for biochemical and biophysical signals that support cell survival, migration and differentiation [29]. The main benefit of decellularised organs or tissues is the presence of three-dimensional fibers and porous topography as well as macroscopic structures like blood vessels, making them ideal scaffolding materials for tissue regeneration. Despite various ECM analogues such as synthetic scaffolds and natural biopolymers [30] have been extensively investigated for tissue engineering, they all exhibit a deficiency in terms of abundant growth factor substances. In order to address this limitation, the decellularization process has been developed to eliminate existing cells from the ECM, thereby eliminating potential antigens that could trigger inflammatory responses and immune-mediated rejection. However, it is worth noting that during the process of decellularization, the existing cells were eliminated, but the growth factors remain preserved. As a result, the extracellular matrix (ECM) derived from decellularised organs showed great potential as a material for tissue engineering.

Type I collagen is the predominant protein in the cardiac environment, while elastin plays a crucial role in the cardiac extracellular matrix (ECM) by facilitating its elastic properties. Both of these proteins are significant components of the hybrid electrospun sheet, contributing to its favorable mechanical and biological characteristics. However, our results also revealed that cardiac patch composed of PCL did not induce cell differentiation of BMMNCs due to the absence of multiple cytokines. Although NP/PCL containing collagen and elastin, which also failed to promote cardiac differentiation. In contrast, hHVS derived from decellularised heart valves still had some of the cytokines present, which are critical for inducing cardiac differentiation. Compared with seeded onto NP/PCL, BMMNCs on hHVS had 253 genes up regulated and 189 genes down regulated. The up-regulated specific differential genes primarily associated with cell proliferation, heart morphogenesis, vasculogenesis, cell adhesion, coronary vasculature morphogenesis, and lysosome organization. Conversely, the down-regulated specific differential genes were mainly enriched in steroid biosynthetic process.

This finding provided a valuable avenue for future research, wherein the incorporation of refined elements into the heart patch can enhance the cardiac differentiation of cells, thereby facilitating a closer resemblance to the heart microenvironment and consequently augmenting its therapeutic efficacy.

Previous investigations had demonstrated a correlation between the study of angiogenic pathways and various cellular processes such as angiogenesis, cell proliferation, cell adhesion, and cell migration [31,32]. Angiogenesis, the formation of new blood vessels, plays a crucial role in both growth and development as well as wound healing. Inflammation serves as a defensive cellular reaction to pathogens, infection, or tissue injury, necessitating intricate molecular signaling to facilitate communication among various immune cells and blood vessels. This biological process can give rise to fever, cardiovascular lesions, allergic sensitization, fibrosis, and autoimmunity, particularly in the context of myocardial ischemia-reperfusion injury repair [33]. Research had demonstrated that MMP9 and TNFα function as detrimental factors in myocardial damage, whereas TIMP1 exerted a notable cardioprotective influence [34]. HGF activates Bcl-2 gene expression and inhibits the translocation of Bax protein to the mitochondrial membrane surface, maintaining the electrochemical gradient inside and outside the mitochondrial membrane and preventing the leakage of cytochrome *c* from the mitochondria, thereby inhibiting the activity of caspase-3 and caspase-9, the apoptosis-related proteins, and producing anti-apoptotic effects [35]. The intricate interplay between residual proteins, encompassing both detrimental and protective elements, is multifaceted. Residual vascular-associated proteins have the potential to foster the development of microcirculation, while residual immune factors can serve as anti-inflammatory agents. The presence of these residual proteins facilitates the emulation of a comparable microenvironment. Matrix metalloproteinases represent the foremost proteolytic system responsible for the degradation of extracellular matrix constituents. They contribute to tissue remodeling by regulating the synthesis of matrix elements and the release of various bioactive factors that facilitate collagen synthesis and the formation of connective tissue with abnormal structure and function, ultimately leading to tissue remodeling and promoting cell differentiation [36]. The primary cause of myocardial damage resulting from myocardial infarction is the disturbance of cardiac microenvironment homeostasis and excessive production of specific pro-inflammatory cytokines. However, these cytokines also play a crucial role in preserving the normal myocardial microenvironment. Our research has revealed that cardiac patches derived from natural tissues exhibit superiority over synthetic cardiac patches in all aspects. This can primarily be attributed to the challenges faced by synthetic cardiac patches in replicating the microenvironment of a healthy heart. Our study has identified that the incorporation of specific cytokines, as discovered in this research, can enhance the ability of synthetic cardiac patches to mimic the normal state of the heart. However, we didn't make sure which one or several cytokines were the best for simulating the cardiac microenvironment. In future study, cardiac repairing can be improved by the addition of appropriate cytokines which were found in this research and more new materials can be applied for myocardial injury repairing.

5. Conclusion

Both cellular materials seeded with BMMNCs mimicked an effective cardiac microenvironment, while hHVS from seeded cells was more effective in improving myocardial function. The reason why hHVS was better than NP/PCL as a scaffold for BMMNCs might be because the optimized method of decellularization let more cytokines in ECM retained.

Ethics declarations

This study was reviewed and approved by Nantong University ethics committee, with the approval number: [S20220611-903].

Data availability

The original data has been uploaded to the GEO database. Data was uploaded in series GSE250573.

Funding

This work was supported by the National Natural Science Foundation of China, China (81770266 and 81300088), "Six-one" Project for High-level Health Talents in Jiangsu, China (LGY2016037), and Jiangsu Postdoctoral Research Funding Program, China (2019K158), Nantong Science and Technology Program, China (JCZ19126).

CRediT authorship contribution statement

Yao Chen: Writing – original draft, Conceptualization. **Zhanghao Huang:** Writing – original draft, Formal analysis, Data curation. **Cheng Ji:** Formal analysis, Data curation. **Jia-Hai Shi:** Writing – review & editing, Writing – original draft, Validation, Funding acquisition, Formal analysis, Data curation, Conceptualization.

Declaration of competing interest

The authors declare that they have no known competing financial interests or personal relationships that could have appeared to influence the work reported in this paper.

Abbreviation

AMI	acute myocardial infarction
BMMNCs	bone marrow mononuclear cells
DEGs	differential genes
DMEM	dulbecco's modified eagle medium
EF	ejection fraction
ECM	extracellular matrix
FS	fraction shortening
GO	gene ontology
GSEA	gene set enrichment analysis
HFIP	hexafluoroisopropanol
hHVS	human heart valve-derived scaffold
KEGG	Kyoto encyclopedia of genes and genomes
LDA	left descending artery
NES	normalized enrichment score
NP	nature protein
PCA	principal component analysis
PCL:	polycaprolactone (abbreviation for nature protein/polycaprolactone (NP/PCL) in article)
PPI	protein-protein interaction
PVC	Pressure-Volume Conductance Catheter System
SDS	sodium dodecyl sulfate
SEM	scanning electron microscope
SPF	specific pathogen-free
TTC	triphenyltetrachloride
WCA	water contact angle

Appendix A. Supplementary data

Supplementary data to this article can be found online at https://doi.org/10.1016/j.heliyon.2024.e31821.

References

[1] S.D. Prabhu, N.G. Frangogiannis, The biological basis for cardiac repair after myocardial infarction: from inflammation to fibrosis, Circ. Res. 119 (1) (2016) 91–112, https://doi.org/10.1161/CIRCRESAHA.116.303577.

[2] Y. Zhu, W. Yang, H. Wang, F. Tang, Y. Zhu, Q. Zhu, et al., Hypoxia-primed monocytes/macrophages enhance postinfarction myocardial repair, Theranostics 12 (1) (2022) 307–323, https://doi.org/10.7150/thno.63642.

[3] A. Kaveh, F.A. Bruton, M.E.M. Oremek, C.S. Tucker, J.M. Taylor, J.J. Mullins, et al., Selective Cdk9 inhibition resolves neutrophilic inflammation and enhances cardiac regeneration in larval zebrafish, Development 149 (8) (2022), https://doi.org/10.1242/dev.199636.

[4] C. Curato, S. Slavic, J. Dong, A. Skorska, W. Altarche-Xifro, K. Miteva, et al., Identification of noncytotoxic and IL-10-producing CD8+AT2R+ T cell population in response to ischemic heart injury, J. Immunol. 185 (10) (2010) 6286–6293, https://doi.org/10.4049/jimmunol.0903681.

[5] K.C. Wollert, H. Drexler, Cell therapy for the treatment of coronary heart disease: a critical appraisal, Nat. Rev. Cardiol. 7 (4) (2010) 204–215, https://doi.org/10.1038/nrcardio.2010.1.

[6] L. Wan, Y. Chen, Z. Wang, et al., Human heart valve-derived scaffold improves cardiac repair in a murine model of myocardial infarction, Sci. Rep. 7 (2017) 39988, https://doi.org/10.1038/srep39988.

[7] Y. Liu, Y. Xu, Z. Wang, D. Wen, W. Zhang, S. Schmull, et al., Electrospun nanofibrous sheets of collagen/elastin/polycaprolactone improve cardiac repair after myocardial infarction, Am J Transl Res 8 (4) (2016) 1678–1694, s2.

[8] L. Lu, J. Ma, Y. Liu, Y. Shao, X. Xiong, W. Duan, et al., FSTL1-USP10-Notch1 signaling Axis protects against cardiac dysfunction through inhibition of myocardial fibrosis in diabetic mice, Front. Cell Dev. Biol. 9 (2021) 757068, https://doi.org/10.3389/fcell.2021.757068.

[9] Q. Zhou, J. Deng, J. Yao, J. Song, D. Meng, Y. Zhu, et al., Exercise downregulates HIPK2 and HIPK2 inhibition protects against myocardial infarction, EBioMedicine 74 (2021) 103713, https://doi.org/10.1016/j.ebiom.2021.103713.

[10] Y. Xu, X. Hu, L. Wang, Z. Jiang, X. Liu, H. Yu, et al., Transplantation of preconditioned bone marrow mononuclear cells by AT2R stimulation improves infarcted heart function via enhanced cardiac mobilization of implanted cells, Int. J. Cardiol. 168 (4) (2013) 4551–4554, https://doi.org/10.1016/j.ijcard.2013.06.087.

[11] D. Maric, A. Paterek, M. Delaunay, I.P. Lopez, M. Arambasic, D. Diviani, A-kinase anchoring protein 2 promotes protection against myocardial infarction, Cells 10 (11) (2021), https://doi.org/10.3390/cells10112861.

[12] Y. Ma, Y. Kuang, W. Bo, Q. Liang, W. Zhu, M. Cai, et al., Exercise training alleviates cardiac fibrosis through increasing fibroblast growth factor 21 and regulating TGF-beta1-smad2/3-MMP2/9 signaling in mice with myocardial infarction, Int. J. Mol. Sci. 22 (22) (2021), https://doi.org/10.3390/ijms222212341.

[13] D. Lv, M. Luo, Z. Cheng, R. Wang, X. Yang, Y. Guo, et al., Tubeimoside I ameliorates myocardial ischemia-reperfusion injury through SIRT3-dependent regulation of oxidative stress and apoptosis, Oxid. Med. Cell. Longev. 2021 (2021) 5577019, https://doi.org/10.1155/2021/5577019.

[14] G.R. Borges, M. de Oliveira, H.C. Salgado, R Jr Fazan, Myocardial performance in conscious streptozotocin diabetic rats, Cardiovasc. Diabetol. 5 (2006) 26, https://doi.org/10.1186/1475-2840-5-26.

[15] A.F. Leite-Moreira, Current perspectives in diastolic dysfunction and diastolic heart failure, Heart 92 (5) (2006) 712–718, https://doi.org/10.1136/hrt.2005.062950.

[16] F. Rostamzadeh, M. Shadkam-Farrokhi, S. Jafarinejad-Farsangi, H. Najafipour, Z. Ansari-Asl, M. Yeganeh-Hajahmadi, PEGylated graphene quantum dot improved cardiac function in rats with myocardial infarction: morphological, oxidative stress, and toxicological evidences, Oxid. Med. Cell. Longev. 2021 (2021) 8569225, https://doi.org/10.1155/2021/8569225.

[17] P. Pacher, T. Nagayama, P. Mukhopadhyay, S. Batkai, D.A. Kass, Measurement of cardiac function using pressure-volume conductance catheter technique in mice and rats, Nat. Protoc. 3 (9) (2008) 1422–1434, https://doi.org/10.1038/nprot.2008.138.

[18] Y. Wang, X. Zhang, M. Duan, C. Zhang, K. Wang, L. Feng, et al., Identification of potential biomarkers associated with acute myocardial infarction by weighted gene coexpression network analysis, Oxid. Med. Cell. Longev. 2021 (2021) 5553811, https://doi.org/10.1155/2021/5553811.

[19] Z. Zhang, S. Ding, X. Yang, J. Ge, Analysis of immune associated Co-expression networks reveals immune-related long non-coding RNAs during MI in the presence and absence of HDC, Int. J. Mol. Sci. 22 (14) (2021), https://doi.org/10.3390/ijms22147401.

[20] J.O. Kim, J.H. Park, T. Kim, S.E. Hong, J.Y. Lee, K.J. Nho, et al., A novel system-level approach using RNA-sequencing data identifies miR-30-5p and miR-142a-5p as key regulators of apoptosis in myocardial infarction, Sci. Rep. 8 (1) (2018) 14638, https://doi.org/10.1038/s41598-018-33020-x.

[21] Z. Wu, X. Huang, M. Cai, P. Huang, Z. Guan, Novel necroptosis-related gene signature for predicting the prognosis of pancreatic adenocarcinoma, Aging (Albany NY) 14 (2) (2022) 869–891, https://doi.org/10.18632/aging.203846.

[22] F. Wu, J. Xu, M. Jin, X. Jiang, J. Li, X. Li, et al., Development and verification of a hypoxic gene signature for predicting prognosis, immune microenvironment, and chemosensitivity for osteosarcoma, Front. Mol. Biosci. 8 (2021) 705148, https://doi.org/10.3389/fmolb.2021.705148.

[23] T. Huang, K. Wang, Y. Li, Y. Ye, Y. Chen, J. Wang, et al., Construction of a novel ferroptosis-related gene signature of atherosclerosis, Front. Cell Dev. Biol. 9 (2021) 800833, https://doi.org/10.3389/fcell.2021.800833.

[24] H.P. Chen, M. Denicola, X. Qin, Y. Zhao, L. Zhang, X.L. Long, et al., HDAC inhibition promotes cardiogenesis and the survival of embryonic stem cells through proteasome-dependent pathway, J. Cell. Biochem. 112 (11) (2011) 3246–3255, https://doi.org/10.1002/jcb.23251.

[25] M.L. Vestergaard, S. Grubb, K. Koefoed, Z. Anderson-Jenkins, K. Grunnet-Lauridsen, K. Calloe, et al., Human embryonic stem cell-derived cardiomyocytes self-arrange with areas of different subtypes during differentiation, Stem Cells Dev 26 (21) (2017) 1566–1577, https://doi.org/10.1089/scd.2017.0054.

[26] M.D. Xia, R.R. Yu, D.M. Chen, Identification of hub biomarkers and immune-related pathways participating in the progression of antineutrophil cytoplasmic antibody-associated glomerulonephritis, Front. Immunol. 12 (2021) 809325, https://doi.org/10.3389/fimmu.2021.809325.

[27] Z.H. Shi, X.Y. Han, M.D. Yao, C. Liu, Q. Jiang, B. Yan, Differential MicroRNA expression pattern in endothelial progenitor cells during diabetic retinopathy, Front. Cell Dev. Biol. 9 (2021) 773050, https://doi.org/10.3389/fcell.2021.773050.

[28] K. Zhu, Q. Wu, C. Ni, P. Zhang, Z. Zhong, Y. Wu, et al., Lack of remuscularization following transplantation of human embryonic stem cell-derived cardiovascular progenitor cells in infarcted nonhuman primates, Circ. Res. 122 (7) (2018) 958–969, https://doi.org/10.1161/CIRCRESAHA.117.311578.

[29] D. Bejleri, M.E. Davis, Decellularized extracellular matrix materials for cardiac repair and regeneration, Adv Healthc Mater 8 (5) (2019) e1801217, https://doi.org/10.1002/adhm.201801217.

[30] H.S. O'Neill, J. O'Sullivan, N. Porteous, E. Ruiz-Hernandez, H.M. Kelly, F.J. O'Brien, et al., A collagen cardiac patch incorporating alginate microparticles permits the controlled release of hepatocyte growth factor and insulin-like growth factor-1 to enhance cardiac stem cell migration and proliferation, J Tissue Eng Regen Med 12 (1) (2018) e384–e394, https://doi.org/10.1002/term.2392.

[31] F. Khodabakhsh, P. Merikhian, M.R. Eisavand, L. Farahmand, Crosstalk between MUC1 and VEGF in angiogenesis and metastasis: a review highlighting roles of the MUC1 with an emphasis on metastatic and angiogenic signaling, Cancer Cell Int. 21 (1) (2021) 200, https://doi.org/10.1186/s12935-021-01899-8.

[32] H.A. Mena, P.R. Zubiry, B. Dizier, V. Mignon, F. Parborell, M. Schattner, et al., Ceramide 1-phosphate protects endothelial colony-forming cells from apoptosis and increases vasculogenesis in vitro and in vivo, Arterioscler. Thromb. Vasc. Biol. 39 (10) (2019) e219–e232, 10.1161/ATVBAHA.119.312766.

[33] T. Zhang, W. Deng, Y. Deng, Y. Liu, S. Xiao, Y. Luo, et al., Mechanisms of ferroptosis regulating oxidative stress and energy metabolism in myocardial ischemia-reperfusion injury and a novel perspective of natural plant active ingredients for its treatment, Biomed. Pharmacother. (2023) 114706, https://doi.org/10.1016/j.biopha.2023.114706.

[34] G. Qiao, W. Ji, Z. Sun, X. Wang, P. Li, H. Jia, et al., Isosteviol reduces the acute inflammatory response after burns by upregulating MMP9 in macrophages leading to M2 polarization, Int Immunopharmacol 106 (2022) 108609, https://doi.org/10.1016/j.intimp.2022.108609.

[35] H. Tang, M. Gamdzyk, L. Huang, L. Gao, C. Lenahan, R. Kang, et al., Delayed recanalization after MCAO ameliorates ischemic stroke by inhibiting apoptosis via HGF/c-Met/STAT3/Bcl-2 pathway in rats, Exp. Neurol. 330 (2020) 113359, https://doi.org/10.1016/j.expneurol.2020.113359.

[36] Y. Arai, S.H. Lee, MMP13-Overexpressing mesenchymal stem cells enhance bone tissue formation in the presence of collagen hydrogel, Tissue Eng Regen Med 20 (3) (2023) 461–471, https://doi.org/10.1007/s13770-023-00535-y.